CONF-961144--1

ATS MATERIALS SUPPORT*

M. A. Karnitz (karnitzma@ornl.gov:423-574-5150)
I. G. Wright (wrightig@ornl.gov:423-574-4451)
M. K. Ferber (ferbermk@ornl.gov:423-576-0818)
R. S. Holcomb (holcomb@ornl.gov:423-574-0273)
Oak Ridge National Laboratory
P. O. Box 2008
Oak Ridge, TN 37831-6065

Mary H. Rawlins (rawlinsmh@ornl.gov:423-576-4507)
U. S. Department of Energy-Oak Ridge
P. O. Box 2008
Oak Ridge, TN 37831-6269

ABSTRACT

The technology based portion of the Advanced Turbine Systems Program (ATS) contains several subelements which address generic technology issues for land-base gas turbine systems. One subelement is the Materials/Manufacturing Technology Program which is coordinated by DOE-Oak Ridge Operations and Oak Ridge National Laboratory (ORNL) for the Department of Energy. The work in this subelement is being performed predominantly by industry with assistance from national laboratories and universities. Projects in this subelement are aimed toward hastening the incorporation of new materials and components in gas turbines.

The materials manufacturing subelement was developed with input from gas turbine manufacturers, material suppliers, government laboratories and universities. Work is currently ongoing on thermal barrier coatings (TBCs), the scale-up of single-crystal airfoil manufacturing technologies, materials characterization and technology information exchange. Westinghouse Power Generation and Pratt & Whitney each have material programs to develop dependable TBCs that enable increased turbine inlet temperatures while maintaining airfoil substrate temperatures at levels to meet the ATS life goals. Howmet and PCC Airfoils each have projects to extend the capability of single-crystal complex-cored airfoil technology to larger sizes so that higher turbine inlet temperatures can be attained in land-based turbines in a cost-effective manner. Materials characterization tasks are ongoing on TBCs in support of the industrial projects. In addition, a project on long-term testing of ceramics and ceramic-matrix composites for gas turbines is being conducted in support of programs at Solar Turbines, Allison Engines, and Westinghouse Power Generation.

OBJECTIVES

The primary objectives of the materials/manufacturing element is to provide materials and material-related manufacturing technology support to the ATS projects and to the gas turbine industry at large. The ATS prime contractors are responsible for the technologies necessary for the demonstration projects. The materials/manufacturing support is intended to complement the ATS team efforts and provide expertise not available to any single contractor.

BACKGROUND INFORMATION

The ATS Materials/Manufacturing Plan was developed in April 1994, (Ref. 1) and focuses on generic materials issues, components and manufacturing processes. The plan was developed in coordination with the turbine manufacturers and

* Research sponsored by U. S. Department of Energy's Office of Energy Efficency and Renewable Energy (Office of Industrial Technologies and Office of Fossil Energy [Morgantown Energy Technology Center]) for the Advanced Turbine Systems Program, Under contract DE-AC05-96OR22464 with Lockheed Martin Energy Research Corporation.

DISCLAIMER

there has been a continuing interaction with the manufacturers since the publication of the plan. The manufacturers have stated a need for turbine inlet temperatures as high as 2600 F to achieve the ATS efficiency goals. To achieve these temperatures for extended operating periods, there is a need to utilize new materials. The turbine manufacturers have also indicated a need for effective interaction among themselves, materials suppliers, national laboratories and others.

The materials/manufacturing subelement has projects underway in four major categories. There are now projects ongoing in coatings and process development, scale-up of single crystal airfoil manufacturing, materials characterization and technology information exchange. This paper summarizes the status of the ongoing activities in these four categories.

PROJECT DESCRIPTION

The coatings and process development program effort is focused on TBCs which, for current systems, involve a ceramic outer layer that provides thermal protection and an inner metallic layer or bond coat. Two projects were initiated in this area; with Westinghouse Power Generation Business Unit of Orlando, Florida and Pratt & Whitney of East Hartford, Connecticut. Both projects were initiated in August 1995. The goal of these programs is the development of dependable TBCs that enable increased turbine inlet temperatures while maintaining airfoil substrate temperatures at levels to meet the ATS life goals. Each of these two projects involves three phases which address:

Phase I - TBC process development,
Phase II - Bench tests,
Phase III - Product line gas turbine testing

These main issues are being addressed by the TBC contractors and by their supporting subcontractors, which include: coating suppliers, universities and national laboratories. Complete descriptions of these projects are addressed in separate papers in these proceedings by Westinghouse and Pratt & Whitney.

Projects are also underway to extend the capability of single-crystal complex-cored airfoil technology to larger sizes, so that higher turbine inlet temperatures can be attained in land-based turbines in a cost-effective manner. Projects are underway with Howmet Corporation in Whitehall, Michigan and PCC Airfoils in Cleveland, Ohio.

The project led by Howmet is supported by a team including; ABB, Pratt & Whitney, Solar Turbines and Westinghouse. The project includes four main thrust areas:

*Low sulfur alloys
*Casting process development and understanding
*Post-casting process development and improvement
*Casting defect tolerance levels

Work on this project has been underway since May 1995. More details on the project is provided in a separate paper in this proceedings by Howmet.

The PCC Airfoils Project is supported by G.E. Power Generation and it also has four major tasks:

*Alloy melt practice
*Modification/improvement of single crystal casting process
*Core material and design
*Grain orientation control

The PCC Airfoils Project was initiated in March 1995 and is described in detail in a separate paper in this proceedings by PCC Airfoils.

There are two main projects under the materials characterization category. One is on long-term testing of ceramics and ceramic matrix composites for gas turbines, the other on TBC characterization. The Department of Energy's Office of Industrial Technologies initiated a program in 1992 to develop ceramic components for use in industrial gas turbines. The program was designed to bring ceramic technologies to the point where short-term reliability and engine performance can be demonstrated. Solar Turbines, Inc. was selected for the development of the ceramic gas turbine components. One of the critical areas outlined in this program was a long-term materials testing program. Long-term

materials testing are needed to determine the survivability of the materials for land-based applications.

As a subset of the Solar Turbines program, ORNL and the University of Dayton Research Institute (UDRI) initiated research activities that focused on the evaluation of the static tensile creep and stress rupture behavior of several commercially available structural ceramics. These materials were identified by the gas turbine manufacturers as leading candidates for use in industrial gas turbines. Because the available information for many candidates structural ceramics was limited to less than 2,000 hours, this project was focused on extending these data to times on the order of 10,000 hours. This time period represents the lower limit of operating time anticipated for ceramic blade and vanes in industrial gas turbine engines.

The TBC Characterization Projects are focused on the development of characterization techniques for the evaluation of the mechanical and thermal reliability of TBCs. An extensive review of the characterization techniques helped focus the program on several of the most promising techniques for further evaluation. Emphasis is being placed upon methods for appropriately measuring of residual stress, thermal conductivity, and damage in the form of micro and macro cracking and oxidation.

The information exchange category of the Materials/Manufacturing element has mainly focused on providing a mechanism for transfer of information on the materials issues developed by other agencies such as: NASA, DoD and DOE materials programs to the ATS Program. Some of these materials efforts have significant impact on the ATS Program. One example of this is a jointly sponsored TBCs workshop that was held with NASA and NIST in Cleveland, Ohio on March 27-29, 1995. A second workshop is planned for May 1997. The objective of these workshops is to assess the state of TBC knowledge and identify critical gaps in knowledge that hinder the use in advanced applications

RESULTS

The results for the coatings and process development projects and the scale-up of singe-crystal blade projects are described in separate papers in this proceedings and are, therefore, not covered in this paper. The results presented in this paper will focus on the materials characterization subelement for both the long-term testing of ceramics and ceramic matrix composites for gas turbines and TBC characterization.

Long Term Testing

Structural ceramics such as silicon carbide and silicon nitride are currently candidates for application as high-temperature components in land-based industrial gas turbines (Refs. 2-4). Metallic components which have been targeted for replacement by these ceramic materials include vanes, blades, shrouds, and combustor liners. The use of ceramics over metallic materials has been stimulated by the potential for higher operating temperatures and thus, higher engine efficiencies. However, because industrial turbines are expected to operate continuously for periods of 30,000+ hours between overhauls, the long-term mechanical reliability of the ceramic components is a major concern. Time-dependent processes such as creep, slow crack growth, oxidation , and cyclic fatigue can result in a continous reduction in the component strength. Premature failure of the component can occur if the strength drops below the maximum service stress.

Efforts to predict the lifetime of ceramic components have been limited by two factors. First, much of the available stress (creep) rupture data describing time-dependent failure is limited to times of 2,000 hours or less. However, in order to assure confidence in the predicted component lives, engine designers have stressed the need for data covering at least 10,000 hours. Second, many of the candidate ceramic materials under consideration are relatively new and thus, little data are available.

This section describes results of a long-term testing program which was initiated in 1992 to address these issues. Research activities in this program focus on the evaluation of the static tensile creep and stress rupture (SR) behavior of three commercially available structural ceramics which have been identified by the gas turbine manufacturers as leading candidates for use in industrial gas turbines. Tensile creep data are being generated in air by measuring creep strain as a

function of time, applied stress, and temperature. The SR resistance is evaluated by continuing each creep test until the specimen fails. For each material investigated, a minimum of three temperatures and four stresses is used to establish the stress and temperature sensitivities of the creep and SR behavior. The test matrix utilized in this program is intended to extend the test conditions investigated by the engine component manufacturers. In the latter case, these conditions focus primarily upon the evaluation of the creep and SR behavior of two candidate materials at one temperature only. Consequently, the temperatures chosen for the this effort bracket those used by the engine component manufacturers. Because existing data for many candidate structural ceramics are limited to testing times less than 2,000 h, this program will focus on extending these data to times on the order of 10,000 h, which represents the lower limit of operating time anticipated for ceramic blades and vanes in gas turbine engines.

Table 1 summarizes the materials that are being examined in the Long-Term Testing project. They include four structural ceramics and one ceramic matrix composite currently being examined in this program. The fabrication of the NT164 is through pressure slip casting for the green state and hot isostatic pressing (HIPing) for the final densification. The microstructure typically consists of β silicon nitride grains having a grain width of less than one micron and an aspect ratio range of 4 to 8. Depending on processing, the α silicon nitride content can range from 5 to 40%. The SA SiC is a sintered silicon carbide which is fabricated in the green-state by injection molding. Additions of small amounts of carbon and boron are used to assist the densification during sintering. Post-sinter HIPing is also used to improve density and reduce defect size. The microstructure of this material typically consists of α silicon carbide grains ranging in size from 2 to 8 μm. Finally, the SN88 silicon nitride is injection molded followed by gas pressure sintering. Sintering aids include Al_2O_3 and Yb_2O_3.

Two new material systems were integrated into the test program during this fiscal year. The first is a monolithic silicon nitride manufactured by AlliedSignal Ceramic Components and designated as AS800. This material, which is classified as a self-reinforced silicon nitride, has a microstructure similar to that of SN88 and is of interest to both Solar Turbines and Allison Engines. The second material, manufactured by Dupont-Lanxide and designated as SiC/DIMOX, is a composite consisting of CG (Ceramic Grade) Nicalon fibers in a aluminum oxide matrix. The fiber architecture consists of an 8 harness satin weave having either a 0-90° or +/-45° lay-up. To reduce the detrimental effects of oxidation, a duplex boron nitride-silicon carbide coating is applied to the fibers (prior to the formation of the matrix) using chemical vapor deposition. The aluminum oxide matrix is formed via the directed metal oxidation of aluminum (DIMOX process). The SiC/DIMOX material is currently being considered for use as a gas turbine component by Westinghouse.

Table 2 summarizes the types of tests conducted on the five material systems. The establishment of tensile stress rupture data covering times from 1 to 10,000 hours is a key objective for all five materials. The NT164 tensile specimens are also being used to validate a new test method combining dynamic fatigue and interrupted stress rupture. Normally dynamic fatigue is used to quickly assess a material's susceptibility to time-dependent fracture by measuring strength as a function of stressing rate. Although one may utilize this information to generate a stress rupture curve, the confidence in the predicted stress rupture lives can be low particularly at the lower stresses. By conducting dynamic fatigue measurements following a static stress for a fixed exposure time (interrupted stress rupture), one should be able to increase the confidence in the stress rupture curve generated from the dynamic fatigue data. The experimental phase of this work, which is being conducted at the University of Dayton Research Institute, is now complete. The analysis of data is underway and should be finished within the next few months.

Stress rupture testing of the SN88 and SA SiC materials is nearly complete. Figures 1 and 2 illustrate the data obtained to date. In general the susceptibility to time-dependent failure as reflected by the slope of the stress rupture curves is less for the SA SiC. However, a major problem with this material is that its relatively low Weibull modulus results in considerable uncertainty in both the

strength and the rupture time. Consequently during stress rupture testing, many specimens which were subjected to stresses slightly below the average fracture strength failed upon loading. In the case of the SN88, time-dependent strength degradation was evident at all temperatures. The associated mechanism was attributed to the formation of creep cavities and their eventual accumulation into a damage zone originating from the specimen surface (refs. 5 and 6). An example of one such damage zone is shown in the micrograph (left-hand side) in Fig. 3. The surface cracks observed along the gage section (micrograph on right) indicate that damage zone formation occurred throughout the gage volume. While the susceptibility to time-dependent failure is greater for the SN88 than that for the SA SiC, the stress rupture data for the SN88 are generally much more repeatable. Because this behavior leads to a much greater confidence in the prediction of component lifetime, SN88 is considered to be a better candidate for component fabrication.

Figure 4 illustrates the strain-time curves obtained to date for the AS800 material. Figure 5 compares the resulting stress rupture behavior with that obtained for the SN88 material at 1288 and 1350°C. Although limited, the data suggest that the resistance to stress rupture of the AS800 is comparable to that of the SN88. In fact one of the AS800 specimens tested at 1316°C and 250 MPa exceeded the failure time for an SN88 specimen tested at 1288°C at the same stress level. The temperature sensitivity of the stress rupture behavior of the AS800 will be established in subsequent tests such that a more direct comparison is possible.

TBC Characterization

The overall goal of this task is to develop and apply advanced techniques to the characterization of TBCs used in land-base gas turbines. The choice of specific characterization methods were based upon (1) a formal needs assessment conducted as part of the Materials/Manufacturing Program, (2) input from discussions recognized experts, and (3) results from workshops and other meetings (NASA/DOE/NIST TBC Workshop), ATS Materials Workshop (SCERDC), ATS Review Meeting, IGTI Turbo/Expo, etc.). The following efforts were initiated in FY95:

Thermophysical Properties and Thermal NDE
Residual Stress
Thermal Gradient Testing
Oxidation Resistance
Failure Mechanisms.

Progress in each of these areas is discussed below.

Thermophysical Properties and Thermal NDE. The primary goal of this research activity is to develop and apply state-of-the-art characterization and non-destructive evaluation (NDE) techniques to evaluate the thermal reliability, performance and stability of TBCs. Previous studies at ORNL and elsewhere have shown that the microstructure of both air plasma sprayed (APS) and electron beam physical vapor deposition (EB-PVD) zirconia coatings are thermally unstable at and above 1000°C. The lamellar porosity, which exists between slats in the APS coatings, evolves into small spherical pores at high temperatures. This microstructural change results in a coating with a higher thermal conductivity since spherical pores are less effective at impeding heat flow than are thin plate-like pores of equal volume. There is evidence that suggests the starting temperature and rate at which these microstructural changes occurs depends on the impurity levels, particularly low melting point oxides, in the starting powders. Reliable knowledge of the thermal conductivity of a TBC is important in modeling the performance of advanced turbine systems which employ TBC systems.

Several techniques have been employed to study advanced TBC systems. These techniques include xenon and laser flash thermal diffusivity, step-heat flux thermal diffusivity, 3ω thermal spectroscopy, infra-red imaging, and scanning thermal conductivity microscopy (STCM). The flash diffusivity, 3ω thermal spectroscopy, and step-heat flux systems are capable of making measurements on free standing coatings as well as coatings bonded to substrates. Flash diffusivity measurements can be made in vacuum, inert gas, oxidizing or reducing atmospheres up to 1700°C, which is significantly higher than any proposed application temperature for these materials. The 3ω technique is ideally suited for coatings that are too

thin to be measured by the flash technique (thickness < 200μm). Infrared imaging will allow thermal diffusivity mapping of the surface of a coating on test coupons and components as well as detect subsurface damage. The scanning thermal conductivity microscope was developed to study thermal conductivity variations on a microscopic scale. This instrument will provide unique insight into the performance of functionally graded, multilayer, and partially oxidized coatings.

During FY 1996, Westinghouse loaned to the ATS program a series of NDE standards. These standards consist of superalloy blocks with MCrAlY bondcoats. Each sample has a defect purposely manufactured into either the substrate or bondcoat. Types of defects include cracks and debonds. The substrates are Udimet 520 and IN738 alloys. All defects have been well characterized and have been inspected with various NDE techniques by other laboratories. These samples will be examined with a new infrared camera. The short range objective is to develop thermography techniques to detect flaws and damage in turbine components. A possible long range goal would be to develop an automated system to inspect turbine components for quality assurance before, during and after use and following refurbishment. Westinghouse is also participating in ORNL's High-Temperature Material Laboratory (HTML) User Program to further study the effects of thermal aging on TBCs.

Figure 6 shows the thermal image of Westinghouse NDE standard I-8. This standard has been manufactured with a 0.25" delamination between the 0.008" thick MCrAlY bondcoat and the IN738 alloy substrate. Below the debonded area is a crack 0.25" long and 0.021" deep. Both defects were observed in the thermal image taken 0.038 seconds after the surface was illuminated with a flashlamp.

The next step will be to show that these defects can still be observed through a 0.010" thick zirconia thermal barrier coating. Three of the NDE standards will be coated with TBCs. Two of these coatings will be applied with delaminations between the TBC and the bondcoat. One of the TBC/bondcoat delaminations will be placed directly over a bondcoat/substrate delamination. These standards will demonstrate the ability of thermography to identify defects even when these defects exist under other defects. Careful timing will enable the depth of the defects to be identified on actual engine tested hardware.

Residual Stress. The primary goal of this research is to characterize the residual stress state and phases in TBCs, bond coats, interfaces. and substrates at room and elevated temperatures and under applied load. Research activities will apply diffraction techniques to characterize the residual stresses in research grade and industrial specimens. Knowledge of stress and phase gradients is critical for understanding TBC failure which is typically associated with a thermally-grown oxide scale. The room-temperature phases, texture, and residual stresses of the thermally-grown scales within and on the three- and two-layer specimens (i.e., top coat/bond; coat/substrate; and bond coat/substrate) will be determined as a function of time and temperature (ambient and in-situ) and depth. The microstructures of the TBC, bond coat, and substrate in the as-received and heat treated states will be observed using the scanning electron microscopy (SEM). Surface roughness and surface area will be measured by profilometry and Brunauer, Emmet, and Teller (BET). This information will be critical for understanding the contributions of oxide scale growth and sintering of the TBC on stress generation.

Table 3 lists the samples acquired for analysis to date. Currently, there are basically four sets of samples: partially stabilized zirconia (PSZ)-PtAl-René N5; vacuum plasma-sprayed (VPS) NiCrAlY-René N5; uncoated René N5 substrates; and alumina scales.

Phase identification and measurement of residual stresses of the samples listed in Table 3 is ongoing. Table 4 lists the phase identification results to date. Sample D1 contains both tetragonal ($a = 3.62 \pm 0.01$ & $c = 5.27 \pm 0.13$ Å) and cubic ($a = 5.14 \pm 0.01$ Å) phases as well as an unknown. The results for the SB2BC sample series confirms the phases cited by Haynes et al. (Ref. 7) Some difficulty has been encountered with the bare single crystal René N5 substrates (samples N5-A & N5-C) in that no reflections have been observed. Various rocking curves have been performed to no avail. These samples will be revisited at a later date perhaps using a Laue technique.

Crystallographic texture or preferred orientation was evident in the θ-2θ scans from the top coats of samples D1 and D2. Pole figures taken on the cubic (111), (200), (220) and (311) indicated a textured coating while the (531) and (620) polefigures indicated a random coating. Since the deposition temperature for EB PVD coatings is 1000 to 1100 °C (<400 °C for plasma assisted EB PVD) (Ref. 8), it is unclear if the texture of the tetragonal phase should be related to that of the cubic phase. Analysis of the texture will be performed at a later date.

The surface residual stresses, as determined by the $\sin^2\psi$ technique, are listed in Table 5. In this method, layers of material were removed via polishing followed by residual strain measurement using an x-ray diffraction technique. Using the Hauk method(Ref. 9), unstrained interplanar spacings , d_0, were determined at each depth from the strain data. This removed many anomalies in the previously-reported strain data (viz., a large strain normal to the sample surface). Figure 7 shows a plot of the strain-depth data for the as-received sample, D1, calculated with the new d_0 values. The in-plane strains, ε_{11} and ε_{22}, increase compressively as the top coat-bond coat interface is approached. Except for the in-plane shear strain, ε_{12}, near the interface, the shear strains were negligible. Figure 8 provides a comparison with the d_0 values from the as-received and heat treated samples. The data suggest that a concentration gradient of yttrium existed in the as-deposited PSZ and was removed via the heat treatment. Figure 9 shows the residual strain as function of depth for the cubic ZrO_2 phase as a function of depth. The initial in-plane strains are slightly tensile, but become compressive as the interface is approached. Although not shown, SEM micrographs of polished and fractured cross-sections of the as-received sample reveal the columnar nature of the top coat with lots of cracks and/or "vertical porosity."

Sample D3 was quartered. The quarters were labeled -1, -2, -3, and -4 and were then heat treated at 1150°C for 100, 60, 200 and 0 hours, respectively. Similarly, sample D9 was also quartered and labeled. Quarters D9-2 and -3 were crushed to make powder from the top coats. Samples D4, D5, D6, D9-1 and AB-38 were then heat treated at 1150°C for 50, 100, 200, 200 and 200 hours, respectively. The top coat of sample AB-38 did not survive the heat treatment, spalling annularly.

Residual strain as a function of depth was also measured in the sample D3-3 (200 hrs at 1150 °C) using the x-ray diffraction/layer removal technique (see Figures 10 and 11). Comparison of Figures 7 and 10 reveal similar-looking strain profiles, except that the onset of increasing in-plane compressive residual strain occurs at a shallower depth for the heat treated sample. As before, except for the in-plane shear strain, ε_{12}, near the interface, the shear strains in the heat treated sample were also negligible. However, the residual strain profiles for the cubic phase in Figures 9 and 11 are very different. The strain is very tensile in cubic phase after 200 hrs at 1150°C. The origin of this tensile strain is unknown at present. Although not shown, SEM micrographs of polished and fractured cross-sections of the heat treated sample are very similar to those of the as-received indicating no microstructural evidence of sintering. In cross-section, a scale grew at the top coat/bond coat interface from 1 μm in the as-received sample to 4 μm after 200 hrs at 1150°C. In addition to the scale, a region with three layers of "reaction products" appears to form within the (Ni,Pt)Al bond coat. Preliminary SEM examination of this region revealed a plethora of compositional variation. An examination of this region is planned using an electron microprobe.

Thermal Gradient Test System. The useful lifetime of current TBC systems is generally limited by failure along the TBC/bond coating interface. Failure is driven by a combination of thermal-mechanical cycling and deleterious environmental attack by hot gas constituents. An efficient test method is needed to aid in the development and characterization of TBCs under realistic temperature and temperature gradient conditions. The gas turbine industry routinely uses burner rig test methods which employ high velocity gas flames and internally cooled specimens. Laboratory thermal gradient rigs currently under development include an electron beam and CO_2 laser facility. These approaches have been and will continue to be valuable in the development of thermal barrier coating systems. However, the above approaches have high capital or operating

costs and significant safety issues which make it difficult to site them in most laboratory facilities.

A thermal gradient rig more suitable for laboratory use is being developed (Fig. 12). The rig employs an internally cooled tubular specimen. The heat flux is generated by an inductively heated zirconia susceptor concentric with the specimen. The maximum heat flux is greater than 50 W/cm^2. The system will be capable of generating turbine relevant temperatures and temperature gradients through TBC coated superalloy specimens. The rig will feature precise control of the heat flux and forced convection internal cooling. TBC surface temperature, TBC / bond coat interface temperature, and internal surface temperatures will be measured and recorded. Provisions for introducing alternative gas environments are incorporated in the design.

The 20 kW RF power supply was installed. Fabrication of principal components for the thermal gradient test rig is nearing completion. A data acquisition system using LabVIEW software will be dedicated to data logging and analysis. The system will be assembled and made operational in the first quarter of FY 1997.

Oxidation Resistance. One of the features of the alloy manufacturing technology programs is the development of production-scale techniques to reduce the sulfur content of single crystal superalloys to very low levels. This trend is based on laboratory-scale studies (Ref. 10) that used a high-temperature hydrogen annealing treatment to reduce the alloy sulfur level, and showed a significant increase in resistance to spallation of the protective oxide on superalloys when the sulfur content of the alloys was reduced to sub-ppm levels. The maximum resistance to scale spallation was achieved at alloy sulfur levels of approximately 0.2 ppm by weight, and the limiting section thickness for which desulfurization could be achieved in reasonable times by this treatment was approximately 50 μm (0.002 in.). A potential limitation of this approach for the large ATS machine-sized blades is that the very thick root section would require extremely long annealing times that may not be compatible with retaining the desired microstructure in the thinner airfoil sections. Yttrium additions are used to improve scale adherence, and it has been suggested (Ref 11) that Y combines with the sulfur in the melt and prevents its deleterious effect. However, there are practical difficulties in retaining Y in the melt due to its tendency to react with the silica-based molds and cores, which would be exacerbated in the large castings required by ATS machines. The substitution of alumina-based cores reduces this problem, but brings with it attendant difficulties in removing the cores from the castings. The successful development of an in-melt desulfurization process could overcome these problems, while potentially having a small impact on the cost of the castings.

A sensitive measure of the effectiveness desulfurization is the resistance to scale spallation of the alloy in a thermal cycling oxidation test. Results from such tests involving exposure between approximately 30 and 1100°C in static air were conducted on specimens taken from ingots from the PCC Airfoils in-melt and hydrogen annealing desulfurizing trials with one single crystal alloy, René N5 (Y-free). The samples consisted of the non-desulfurized alloy containing 2-3 ppm S; melt-desulfurized alloys with 0.8 to 1 ppm S and 0.4 ppm S; hydrogen-desulfurized alloy (0.8 ppm S); and samples that were desulfurized in-melt followed by hydrogen treatment to give less than 0.3 ppm S. For comparison, the tests included samples of the standard René N5 alloy (3-4 ppm S, 50 ppm Y) and an experimental alloy, NiAl containing 0.03 ppm Zr, which forms an exceptionally adherent alumina scale. The resulting weight change-time curves from weighings every 50 hr of specimens subjected to cycles consisting of 1-hour at temperature are shown in Fig. 13. The non-desulfurized, Y-free alloy exhibited significant scale spallation after only 35 cycles; the scale spalled in small strips. The alloys expected to form adherent scales, N5(Y) and NiAl-Zr, showed the expected weight gains at essentially the same parabolic rates. Of the desulfurized alloys, the kinetic curve for that with less than 0.3 ppm S tracked that for the N5(Y) alloy, whereas the 0.4 ppm S alloy exhibited a lower weight gain; the early kinetics for the alloy with 0.8 to 1.0 ppm S indicated a tendency to weight loss after 100 cycles. The almost flat weight gain curve for the 0.4 ppm S alloy indicated a small level of scale spallation; scale was lost over discrete areas some 30 to 60 μm across which then formed scales containing Ni, Co, and Cr. There appeared to be

some correspondence between the locations of these areas and concentrations of Ta (or W) in the alloy substrate.

Figure 14 compares the oxidation kinetics from these cyclic tests with kinetics from companion isothermal oxidation tests at 1100°C for the non-desulfurized alloy, the alloy desulfurized to 0.4 ppm S, and N5(Y). Taking the difference between the isothermal and kinetic curve for each alloy to represent the extent of scale spallation in the cyclic test, the N5(Y) alloy exhibits essentially perfect adherence under these test conditions, since the curves are coincident. The cyclic oxidation curve for the alloy containing 0.4 ppm S showed some departure from the isothermal curve, signifying some spallation, whereas the curves for the non-desulfurized alloy diverged significantly, and the isothermal oxidation rate for this alloy was faster than for the other alloys, suggesting some contribution from spallation under isothermal conditions.

Similar trends to those shown in Fig. 13 are shown in Fig. 15 for cyclic oxidation at 1100°C with 100 hr between cycles. A further difference between the test conditions was that in the 1-hr cyclic test the specimens were rapidly introduced and withdrawn from a heated furnace, whereas in the 100-hr cyclic tests the specimens were placed in individual alumina crucibles that were placed in a cold furnace before heating, and were furnace cooled. Again, the tendency to scale spallation decreased markedly with decreasing sulfur level. At 0.4 ppm S, spallation was evident after approximately 500 cycles, whereas the <0.3 ppm S alloy showed no signs of spallation at 600 cycles, and was tracking the kinetics of the NiAl-Zr alloy. These data appear to be in good agreement with those from the original laboratory desulfurization experiments using hydrogen annealing, which suggested that the optimum sulfur level for scale adherence was of the order of 0.2 ppm.

Comparison of the kinetic curves in Figs. 13 and 15 indicates that the 0.4 ppm S and N5(Y) alloys, for instance, experienced larger weight gains in the 100-hr cyclic test that in the 1-hr cycles; the weight gains in the 100-hr cycle test also were larger than for isothermal exposures at the same temperature (which involved the rapid introduction of the specimen into a heated furnace). These higher weight gains in the 100-hr cycle test probably are a result of the development of larger amounts of transient oxides during the prolonged initial heating stage, compared to the 1-hr cycle test: any possible effects of differences in stress levels in the scales in the two test conditions on cracking on cooling remain to be resolved. One implication of the differences in scale growth and spallation behavior resulting from different thermal cycles is that the conditions imposed by the duty cycle of ATS engines may lead to oxidation behavior that is different from that which has been well characterized for aircraft engine duty cycles.

Failure Mechanisms. The purpose of this research is to identify failure mode(s), understand and evaluate failure mechanisms, and develop appropriate test methods and protocols to characterize the integrity and predict failure of TBCs during thermal shock and cyclic oxidation.

Evaluation of the elastic modulus of TBCs by the indentation technique is based on the measurement of elastic recovery of the surface impression of the indentation diagonals made by a Knoop indenter. To investigate the applicability of this technique, effects of indentation load and the corresponding indent impression size on the measured elastic modulus of ZrO_2 coatings were evaluated. Results for elastic moduli obtained for different indentation loads are shown in Fig. 16. The measured elastic moduli decreased from a value of 68.4± 22.6 GPa at an indentation load of 50 grams to a value of 37.7 ± 9.8 GPa at an indentation load of 300 grams. Further increase in indentation load did not result in any significant change in the elastic modulus value.

At the lower loads the indentation encompasses only a relatively small region of the TBC. The indentation size is on the order of a single grain or lamella of ZrO_2 coating. This minimizes the extent of defects (such as pores, grain/lamellae boundaries, microcracking, etc.) encompassed by the indentation, which results in observed higher elastic modulus values. On the other hand, at higher loads, the indentation size is large and encompasses many microstructural defects as described above. This results in the observed decrease in elastic modulus. After a critical load is exceeded (300 grams in the present case), the extent of defects encountered per unit area or per unit volume encompassed by the

indentation becomes relatively constant. Therefore, the resulting elastic modulus value becomes insensitive to the indentation load after the critical load is reached. This value can be used for the purpose of materials comparison/selection and design analysis. Furthermore, the measured elastic modulus values (40 to 65 GPa) for the ZrO_2 TBC are much smaller than those reported for fully-dense bulk ZrO_2 (220 GPa). This difference results from the presence of large porosity and microcracks as indicated by microstructural observations.

FUTURE WORK

In the long-term testing effort, future work will focus on the measurement of the creep and stress rupture behavior of additional composites which are of interest to Solar Turbines and Allison Engines. Efforts to evaluate the thermomechanical behavior of TBC systems will also be initiated.

In the areas of thermophysical properties and thermal NDE, thermal diffusivity and conductivity measurements will be made on as-fabricated as well as thermally aged (cycled) coatings. The increases in thermal conductivity due to thermal aging will be modeled as a function of temperature and time at temperature. Thermal conductivity changes will also be correlated with the impurity level of the starting powders. In addition to thermal transport and NDE studies, this task will also investigate the relative thermal expansion of TBCs as a function of temperature, time, and oxidation. These measurements will be made using a custom designed bi-layer dilatometer. Measurements can be made in vacuum, inert gas, or oxidizing atmospheres up to 1650° C.

Results from these thermal conductivity studies will be correlated with microstructural and thermomechanical investigations in order to provide a complete understanding of the factors which affect the performance and life of advanced TBCs. This understanding is a necessary step in the development of comprehensive life prediction models.

In the Residual Stress area, future effort will be placed upon the measurement of strains in TBC systems at elevated temperatures. This will also include the measurement of strains and crystallographic texture in the oxide scale. Finally, the strains as determined from x-ray diffraction will be compared to at least two techniques (Raman spectroscopy , microfluorescence, bilayer dilatometry, and neutron diffraction).

Based on guidance from the gas turbine manufacturers, decisions will be made on whether to proceed with specific characterization techniques. Consideration will also be given to conducting model verification tests in more representative gas turbine environments. This program is also being closely coordinated with related ongoing work at the HTML. This includes an HTML Industrial Fellow Program which is characterizing the thermal stability of EB-PVD TBCs, and the HTML User Program

Future oxidation studies will focus on quantifying the influence of substrates and bond coating sulfur level on the lifetime of TBC systems, and on understanding the reasons for differences in the scale adherence on different alloy-bond coating ceramic combinations.

REFERENCES

(1) E. E. Hoffman, M. A. Karnitz, J. H. DeVan, R. S. Holcomb, D. Anson, R. W. Harrison, R. P. Allen, "Materials/Manufacturing Plan for Advanced Turbine Systems Program", April 1994, DOE-OR-2007

(2) M. van Roode, "Ceramic Retrofit Program," pp. 77-93 in Proceedings of the Joint Contractors Meeting: FE/EE Advanced Turbine Systems Conference FE Fuel Cells and Coal-Fired Heat Engines Conference, DOE/METC-93/6132, August 1993.

(3) M. van Roode, "Ceramic Stationary Gas Turbine Development Program-Third Annual Summary," to be published in the proceedings of ASME Turbo Expo '96 Conference, Birmingham, UK, June 10-13, 1996.

(4) R. Wenglarz, S. Ali, and A. Layne, "Ceramics for ATS Industrial Turbines," to be published in the proceedings of ASME Turbo Expo '96 Conference, Birmingham, UK, June 10-13, 1996.

(5) A. A. Wereszczak, M. K. Ferber, T. P.

Kirkland, M. R. Foley, and R. L. Yeckley, "Evolution of Stress Failure Resulting from Stress/Oxidation Damage in a Hot Isostatically Pressed Silicon Nitride at Elevated Temperatures," *J. Amer. Ceram. Soc.*, **78** [8] 2129-40, 1995.

(6) A. A. Wereszczak, M. K. Ferber, T. P. Kirkland, and K. L More, "Evolution of Oxidation and Creep Damage Mechanisms in HIPed Silicon Nitride Materials," pp. 457-66 in Plastic Deformation of Ceramics, edited by R. C. Bradt, Plenum Press, New York, 1995.

(7) J. A. Haynes, E. D. Rigney, M. K. Ferber, W. D. Porter. "Oxidation and Degradation of a Plasma-Sprayed Thermal Barrier Coating System," in preparation.

(8) K. S. Fancey and A. Mathews, "Ionization Assisted Physical Vapor Deposition of Zirconia Thermal Barrier Coatings," J. Vac. Sci. Technol. A 4 [6] 2656-60 (1986).

(9) I. C. Noyan and J. B. Cohen, *Residual Stress Measurement by Diffraction and Interpretation.* Springer-Verlag, New York, 1987.

(10) J. L. Smialek, D. T. Jayne, J. C. Schaeffer, and W. H. Murphy, Thin Solid Films, 253, 285-292 (1994).

(11) See, for instance, A. W. Funkenbusch, J. G. Smeggil, and N. S. Bornstein, Met. Trans., 16A, 1164 (1985).

ACKNOWLEDGMENT

The technical and program guidance of DOE Energy Efficiency and Renewable Energy Program Managers Patricia Hoffman and Stan Blazewicz and DOE Morgantown Energy Technology Technical Manager, Chuck Alsup is gratefully acknowledged. We are also grateful for the guidance of our gas turbine industry partners.

Table 1. Summary of Tensile and Flexure Specimen Matrix Examined in this Program

Material	Supplier	No. of Tensile Specimens	No. of Flexure Specimens
SA SiC	Carborundum Company Niagara Falls, NY 14302-0832	50	205
SN88 Si_3N_4	NGK Insulators, LTD Nagoya, Japan	50	205
NT164 Si_3N_4	Saint-Gobain/Norton Industrial Ceramics Northboro, MA 01532-1545	126	205
AS800 Si_3N_4	AlliedSignal Ceramic Components	33	0
SiC/DIMOX	Dupont-Lanxide	-**-	

Table 2. Summary of Test Protocol for Each Material System

Material	Test Type	Temperatures (°C)
SA SiC	-Flexural Dynamic Fatigue	1350
	-Tensile Creep	1150
	-Tensile Stress Rupture	1038
SN88 Si_3N_4	-Flexural Dynamic Fatigue	1350
	-Tensile Creep	1150
	-Tensile Stress Rupture	1038
NT164 Si_3N_4	-Flexural Dynamic Fatigue	1350
	-Combined Dynamic and Interrupted Stress Rupture	1150
		1038
AS800 Si_3N_4	-Tensile Creep	1316
	-Tensile Stress Rupture	990
SiC/DIMOX	-Tensile Creep	1000
	-Tensile Stress Rupture	1100
	-Stress Relaxation	1200

Table 3. Summary Of Samples Acquired Through 7/96

Sample ID	Top Coat	Bond Coat	Substrate	Layer Thicknesses (mm)	Conditions or Notes
D1 - D9	EB PVD PSZ *	PtAl	René N5	0.37-0.05-1.6	As-received & thermally treated
AB-38, AB-39	EB PVD PSZ *	PtAl	René N5	?	As-received
SB2BC01, 02, 03, 04	none	VPS NiCrAlY †	René N5	0.15-3.18	Oxidized @ 1150°C for 100, 200, 50, and 100 hr, respectively
1 hour NiCrAlY	none	VPS NiCrAlY	René N5	0.15-3.18	Oxidized @ 1150°C for 1 hour
BC-1	none	PtAl	René N5	0.05-3.16	As-received
N5-1	none	none	René N5	3.20	As-received
N5-A	none	none	René N5	1.8	As-received, 3 ppm sulfur
N5-C	none	none	René N5	1.3	As-received, 0.4 ppm sulfur
APM	none	none	FeCrAl+ZrO_2	?	Oxidized @ 1200°C for 1000 hr
NA7Z	none	none	NiAl+Zr	?	Oxidized @ 1200°C for 1000 hr

* Electron beam physical vapor deposited partially stabilized zirconia = 7-8 wt% Y_2O_3-ZrO_2
† Vacuum plasma-spray Ni-22Cr-10Al-1Y (wt%)

Table 4. Summary Of The Phases In The Surface Region Of The Samples

Sample ID	Phases	Content	ICDD Card #	Testing condition
D1	t-Y_2O_3-ZrO_2	Major	38-1437	As-received
	c-Y_2O_3-ZrO_2	Major	30-1468	
	unknown	Minor		
D2	dtba *			As-received & oxidized @ 1200°C for 72 hr
D3	untested			As-received & oxidized @ 1150°C for 60, 100, 200 hr
UC1, UC2	untested			As-received
SB2BC01	α-Al_2O_3	Major	43-1484	Oxidized @ 1150°C for 100 hr
	$NiAl_2O_4$	Major	10-0339	
	$Al_{0.1}Ni_{0.9}$	Major	44-2287	
	Y_2O_3	Minor	43-1036	
	$Y_3Al_5O_{12}$	Minor	09-0310	
	NiO	Minor	04-0835	
	$AlYO_3$	Minor	33-0041	
SB2BC02	same as SB2BC01			Oxidized @ 1150°C for 200 hr
SB2BC03	same as SB2BC01			Oxidized @ 1150°C for 50 hr
SB2BC04	same as SB2BC01			Polished then oxidized @ 1150°C for 100 hr
BC-1	dtba *			As-received
N5-1	untested			As-received
N5-A	npo **			As-received, 3 ppm sulfur
N5-C	npo **			As-received, 0.4 ppm sulfur
APM	untested			Oxidized @ 1200°C for 1000 hr
NA7Z	untested			Oxidized @ 1200°C for 1000 hr

* dtba = data to be analyzed; ** npo = no peaks observed during initial scans

Table 5. Summary Of The Residual Stresses In The Surface Region Of The Samples

Sample ID	(hkl) Phase	Residual Stress (MPa) (± 10 MPa)	Residual Strain (ppm)	Testing condition
D1	(403) t-PSZ	5	15	As-received
	(332) t-PSZ	40	500	As-received
D2	(403) t-PSZ	-9	-170	As-received
	(332) t-PSZ	6	90	As-received
SB2BC01	(416) α-Al_2O_3	dtba *		Oxidized @ 1150°C for 100 hr
SB2BC02	(416) α-Al_2O_3	-290	-560	Oxidized @ 1150°C for 200 hr
SB2BC03	(416) α-Al_2O_3	dtba		Oxidized @ 1150°C for 50 hr
SB2BC04	(416) α-Al_2O_3	dtba		Polished then oxidized @ 1150°C for 100 hr
BC-1	PtAl	-680	-2040	As-received

* dtba = data to be analyzed

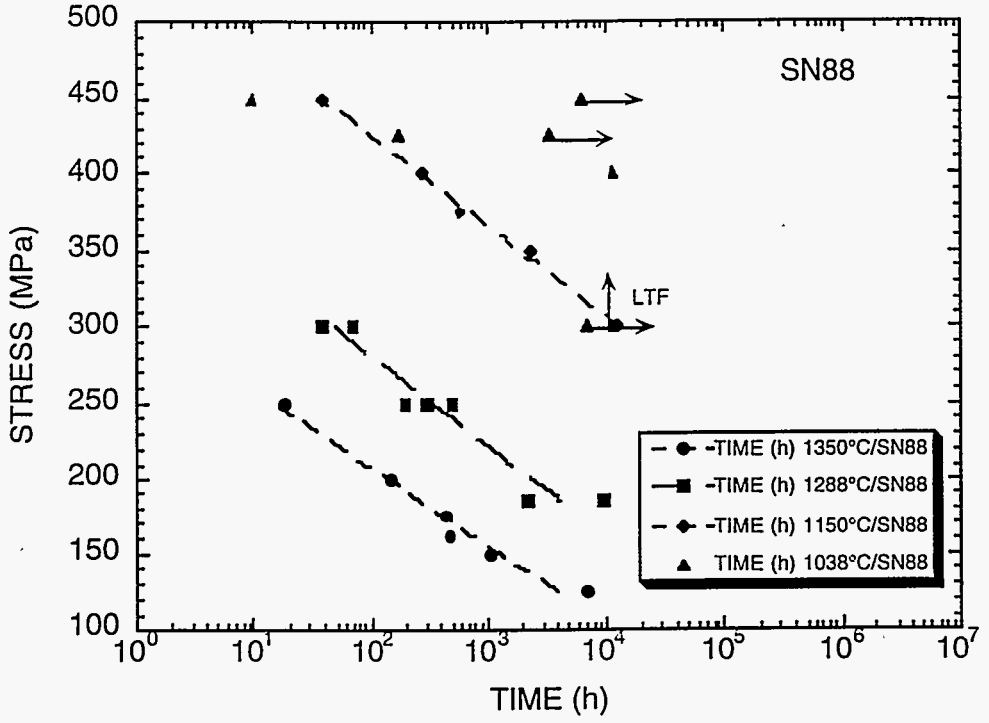

Figure 1. Stress Rupture Data Obtained To Date For The SN88 Silicon Nitride

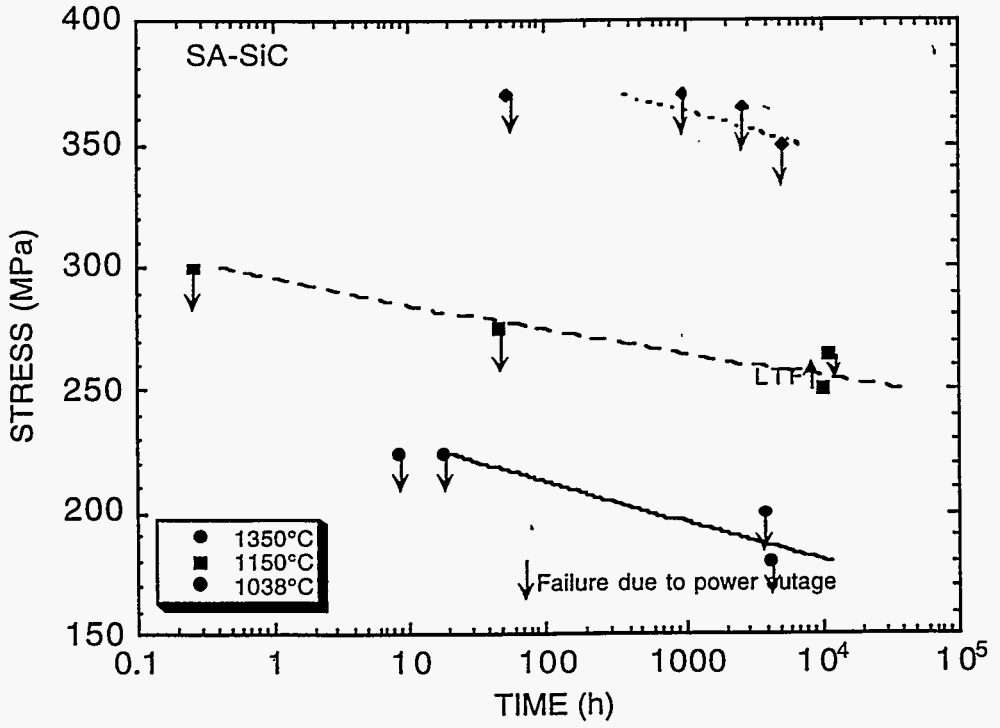

Figure 2. Stress Rupture Data Obtained To Date For The SA SiC Silicon Carbide

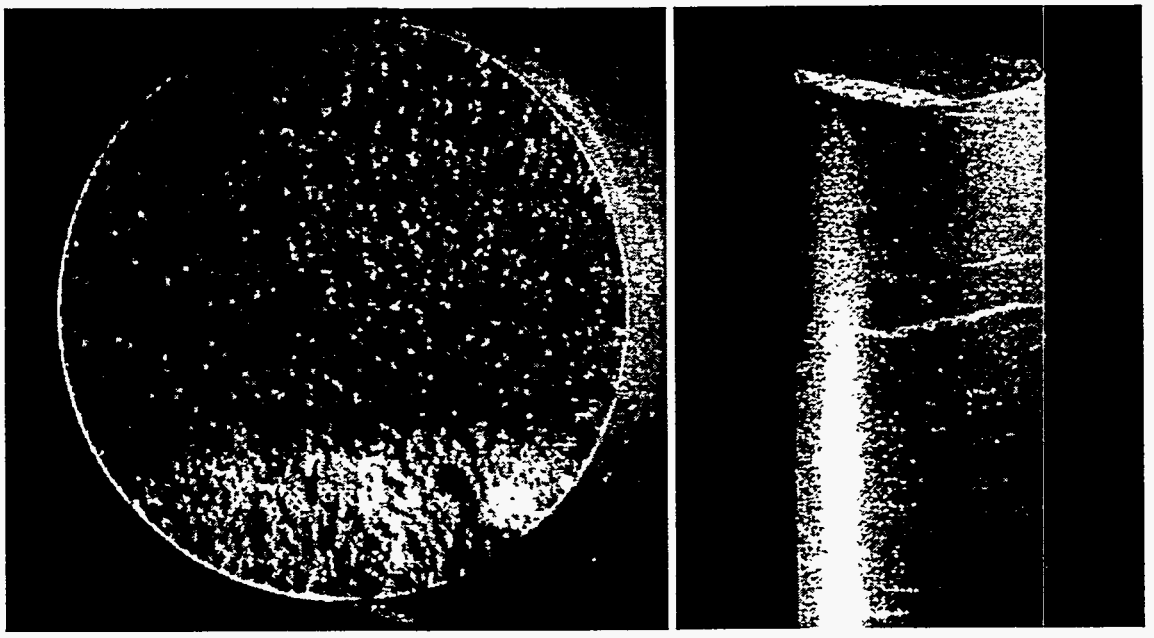

Figure 3. Fracture Characteristics Of SN88 Specimen Tested At 1350°C And 125 Mpa

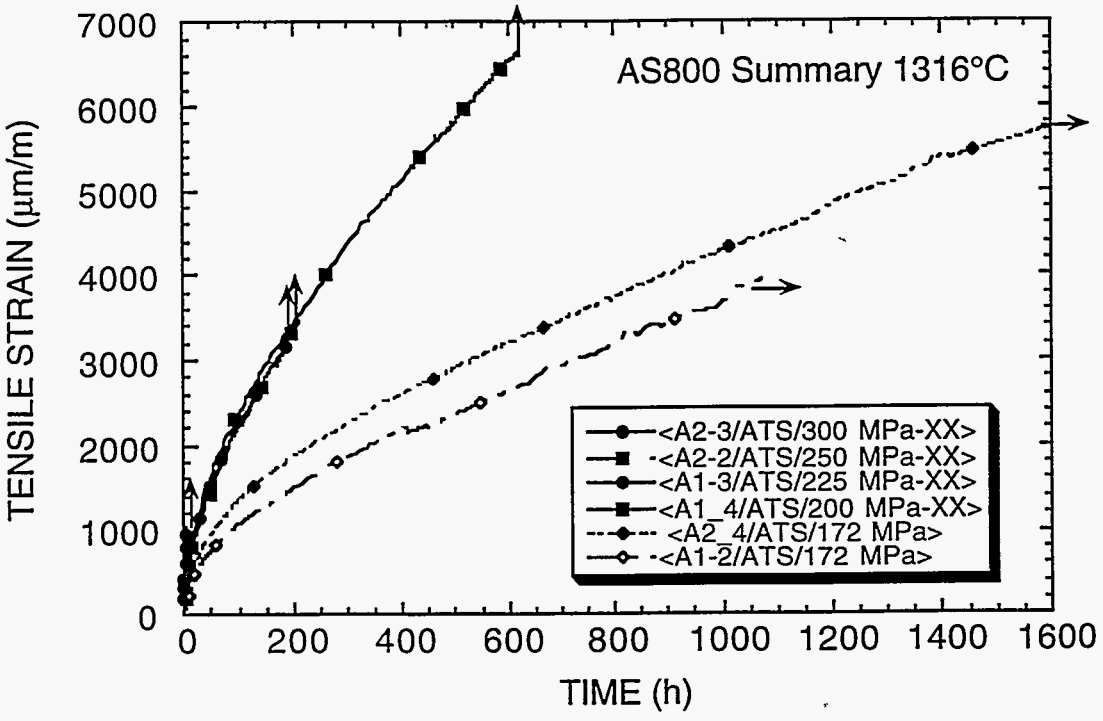

Figure 4. Strain-Time Data Collected For The AS800 At 1316°C

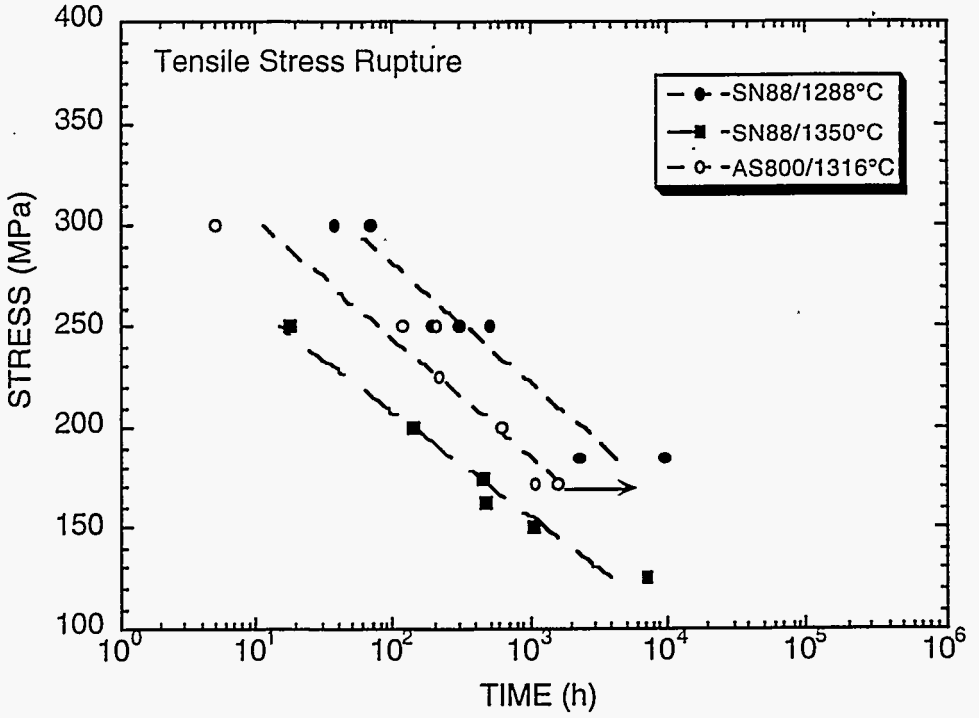

Figure 5. Comparison Of The Stress Rupture Data Obtained For The AS800 At 1316°C And The SN88 At 1288 And 1350°C

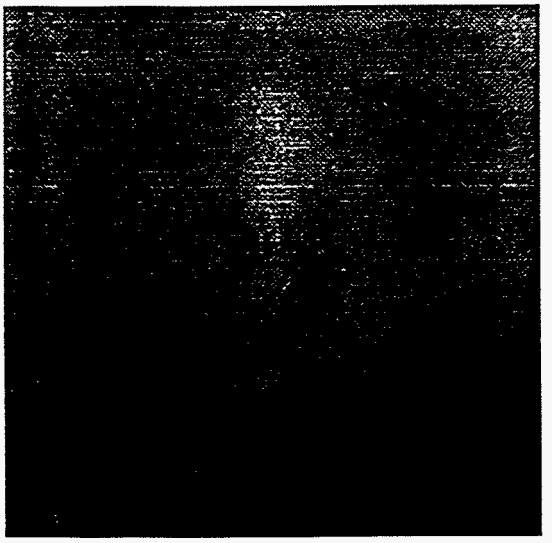

Figure 6. Thermal Image Taken Of Sample I-8, 0.038 Seconds After Flash

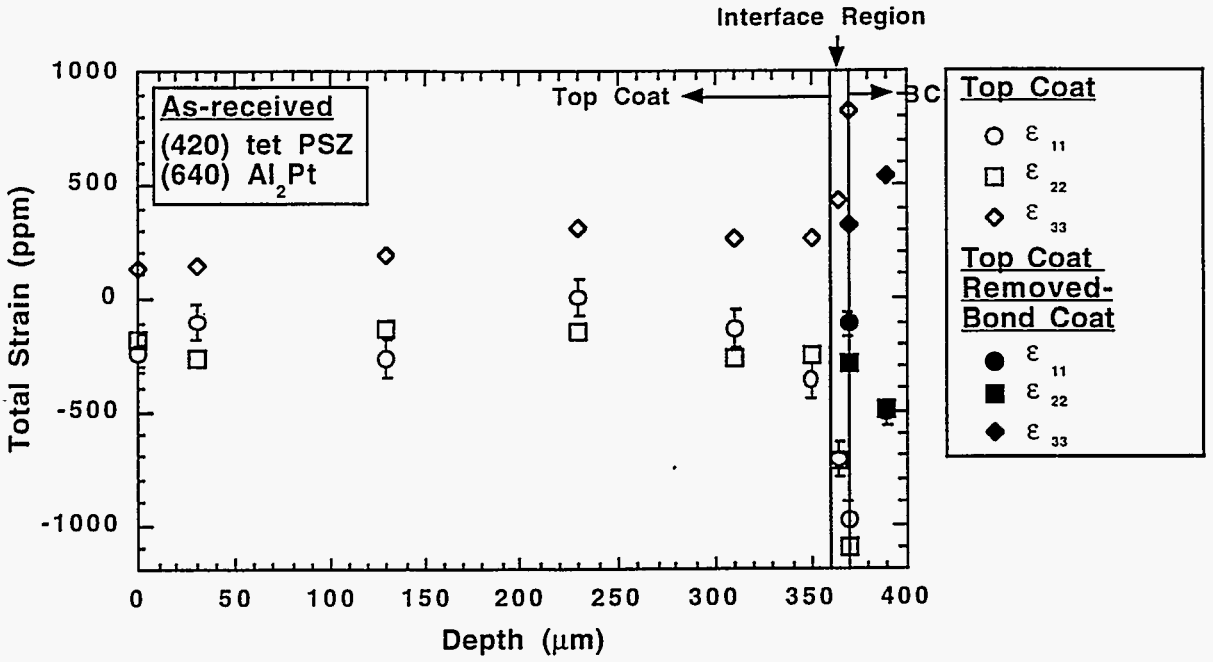

Figure 7. Depth Profile Of Residual Strain In The Tetragonal Phase Of Sample D1 Via X-Ray Diffraction/Layer Removal Technique

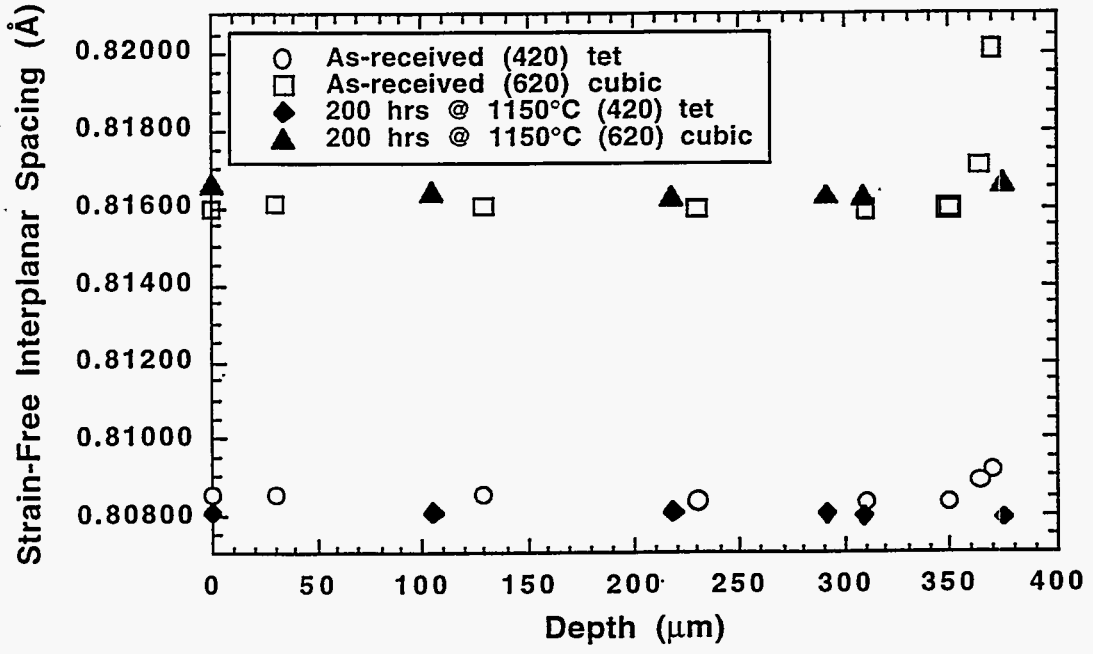

Figure 8. Depth Profile Of Strain-Free Interplanar Spacings For The As-Received And Heat Treated Samples, D1 And D3-3, Respectively

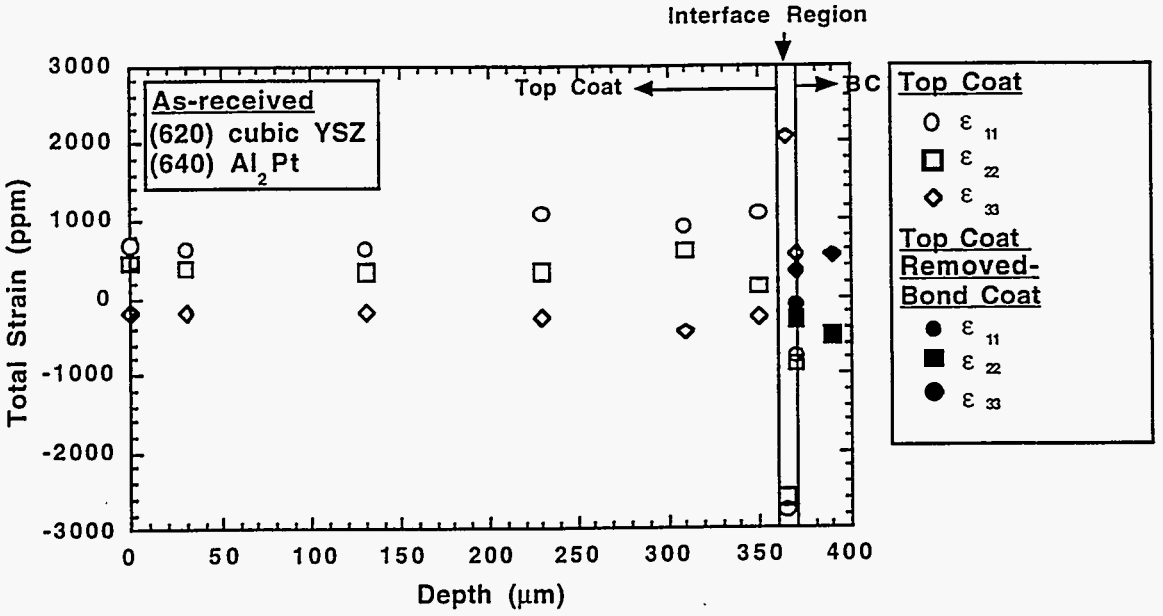

Figure 9. Depth Profile Of Residual Strain In The Cubic Phase Of Sample D1 Via X-Ray Diffraction/Layer Removal Technique

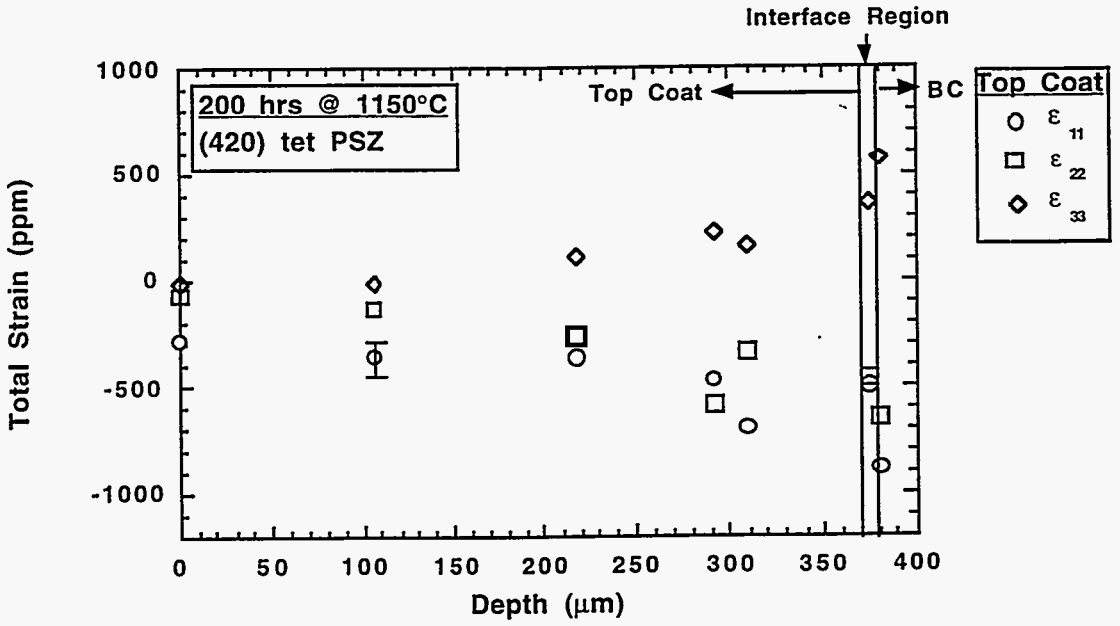

Figure 10. Depth Profile Of Residual Strain In The Tetragonal Phase Of Sample D3-3 Via X-Ray Diffraction/Layer Removal Technique

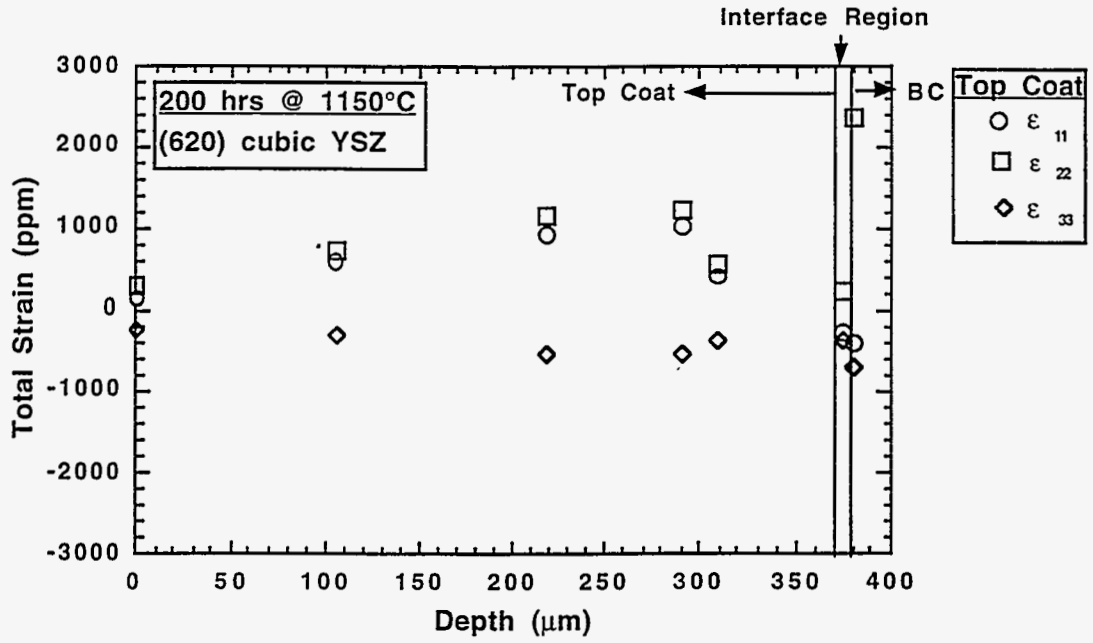

Figure 11. Depth Profile Of Residual Strain In The Cubic Phase Of Sample D3-3 Via X-Ray Diffraction/Layer Removal Technique

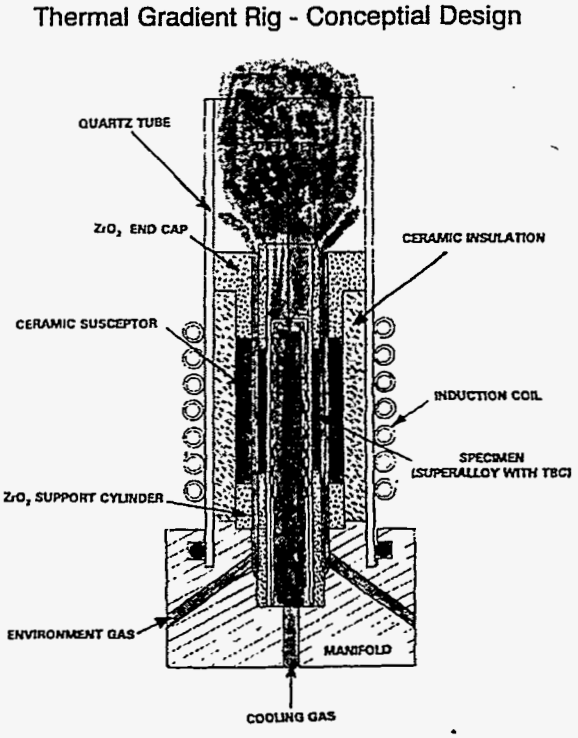

Figure 12. Schematic Representation Of The Proposed Thermal Gradient Test Facility

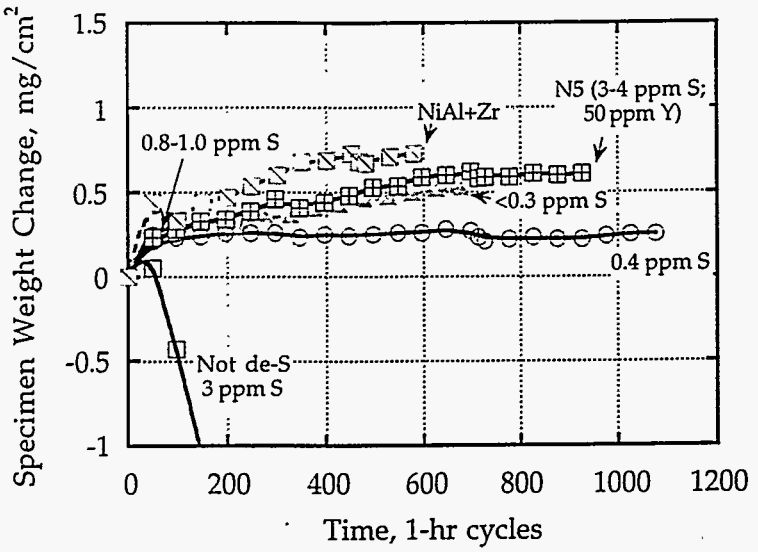

Figure 13. Cyclic Oxidation Kinetics (1 Hr At Temperature) For Ni-Base Superalloy René N5 At 1100°C In Air, Showing Effects Of Desulfurization

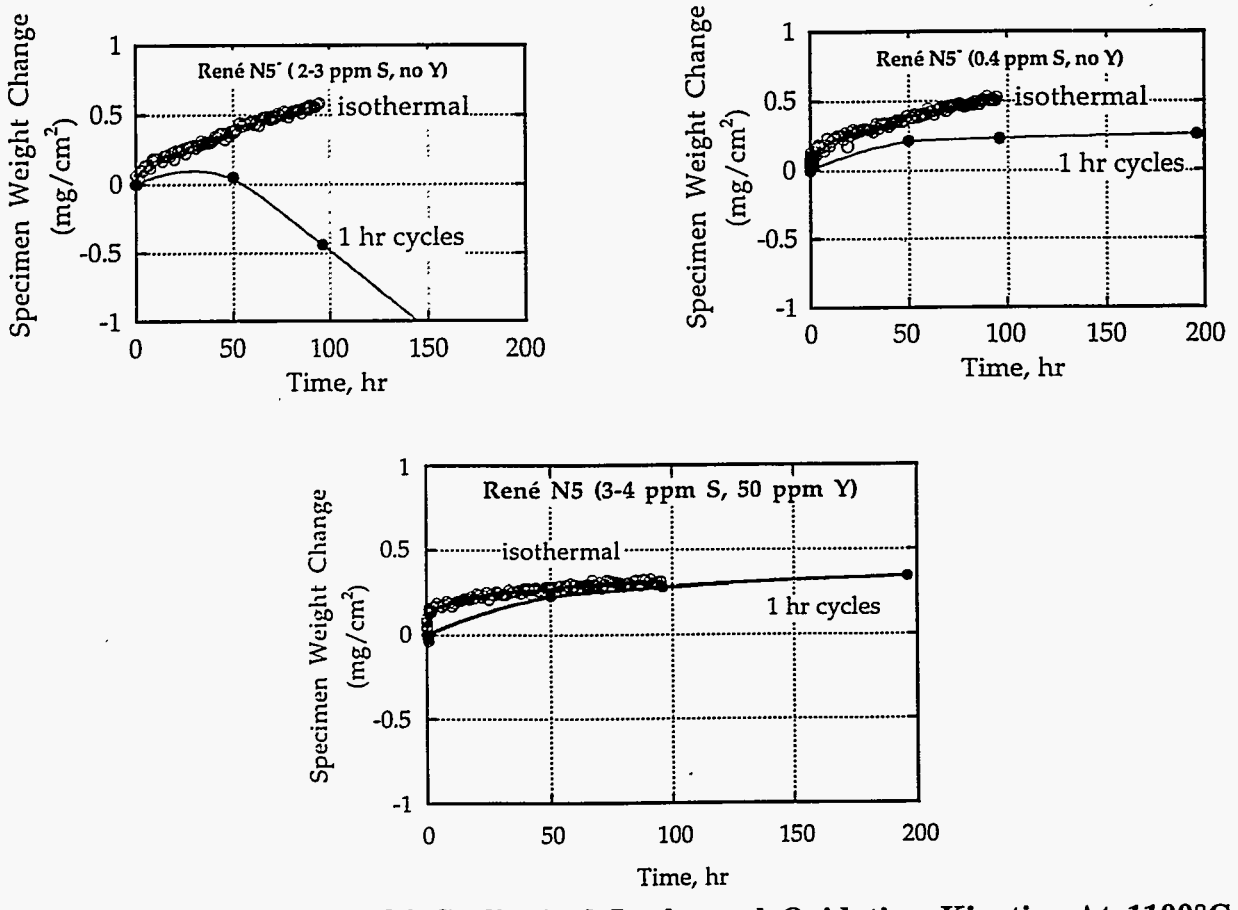

Figure 14. Comparison Of Cyclic And Isothermal Oxidation Kinetics At 1100°C

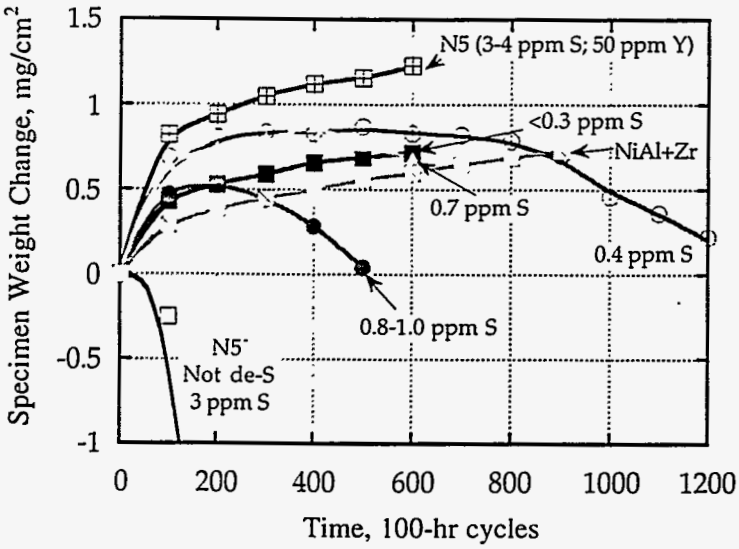

Figure 15. Cyclic Oxidation Kinetics (100 Hr At Temperature) For René N5 At 1100°C In Air, Showing Effects Of Desulfurization

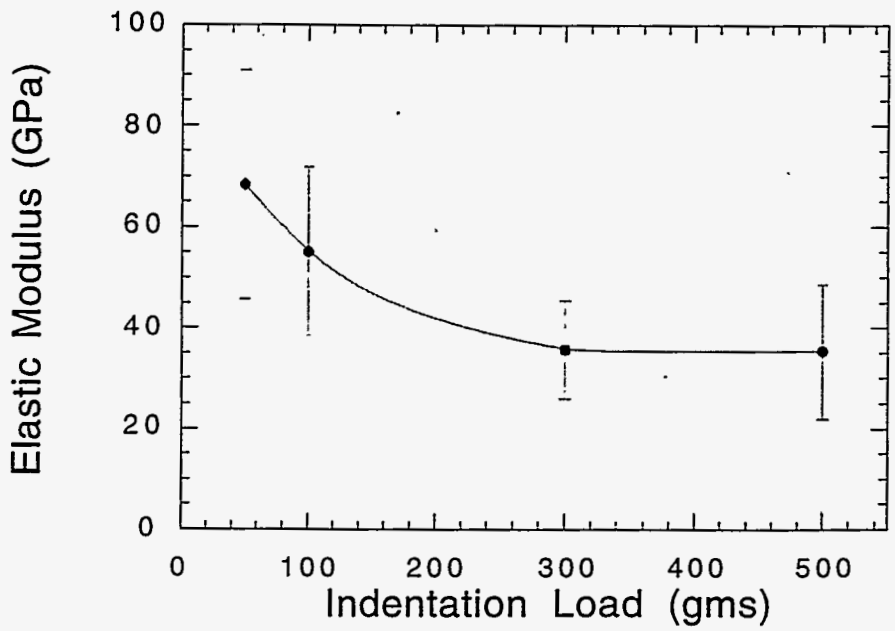

Figure 16. Dependence Of Measured Elastic Modulus Of APS ZrO_2 Coatings On Indentation Load